

## RESEARCH ARTICLE

10.1029/2017JD027795

## Key Points:

- An I-HARLS AOD retrieval algorithm (1 km) for MODIS images is proposed over land
- I-HARLS AOD retrievals agree well with AERONET AOD measurements over land
- I-HARLS AOD retrievals are overall better and less biased than MOD04\_3K AOD products

## Supporting Information:

- Supporting Information S1

## Correspondence to:

L. Sun and Y. Peng,  
sunlin6@126.com;  
pyiran@mail.tsinghua.edu.cn

## Citation:

Wei, J., Sun, L., Peng, Y., Wang, L., Zhang, Z., Bilal, M., & Ma, Y. (2018). An improved high-spatial-resolution aerosol retrieval algorithm for MODIS images over land. *Journal of Geophysical Research: Atmospheres*, 123, 12,291–12,307. <https://doi.org/10.1029/2017JD027795>

Received 26 SEP 2017

Accepted 16 OCT 2018

Accepted article online 22 OCT 2018

Published online 10 NOV 2018





## Author Contributions:

**Data curation:** Yanci Ma**Validation:** Jing Wei**Writing - original draft:** Jing Wei**Writing - review & editing:** Jing Wei,

Lin Sun, Yiran Peng, Lunche Wang,

Zhaoyang Zhang, Muhammad Bilal

## An Improved High-Spatial-Resolution Aerosol Retrieval Algorithm for MODIS Images Over Land

Jing Wei<sup>1,2</sup> , Lin Sun<sup>3</sup>, Yiran Peng<sup>2</sup>, Lunche Wang<sup>4</sup> , Zhaoyang Zhang<sup>5</sup> , Muhammad Bilal<sup>6</sup> , and Yanci Ma<sup>3</sup>

<sup>1</sup>State Key Laboratory of Earth Surface Processes and Resource Ecology, College of Global Change and Earth System Science, Beijing Normal University, Beijing, China, <sup>2</sup>Ministry of Education Key Laboratory for Earth System Modeling, Department of Earth System Science, Tsinghua University, Beijing, China, <sup>3</sup>College of Geomatics, Shandong University of Science and Technology, Qingdao, China, <sup>4</sup>School of Geography and Information Engineering, China University of Geosciences, Wuhan, China, <sup>5</sup>College of Geography and Environmental Sciences, Zhejiang Normal University, Jinhua, China, <sup>6</sup>School of Marine Sciences, Nanjing University of Information Science and Technology, Nanjing, China

**Abstract** MODerate resolution Imaging Spectroradiometer (MODIS) data can play an important role in aerosol retrieval at the global scale due to their short revisit period and long-term observations. The operational MODIS aerosol optical depth (AOD) products are severely limited in air quality studies at the city or local scales due to their coarse spatial resolutions. Therefore, an improved aerosol retrieval algorithm for MODIS images at 1-km spatial resolution is proposed in this paper. This algorithm is based on the high-resolution aerosol retrieval algorithm with a priori land surface reflectance database support (HARLS), which was developed over bright urban areas and was subsequently modified and validated over land. For this study, an eight-day surface reflectance database and a seasonal aerosol-type database over land are constructed using the MODIS surface reflectance and aerosol products. Four typical regions (in Europe, North America, Beijing-Tianjin-Hebei, and the Sahara) with different underlying surfaces and aerosol types are selected to perform the aerosol retrieval experiments. The AOD retrievals are validated against the AEROSOL RObotic NETwork (AERONET) version 2 level 2.0 AOD measurements and compared with the operational MODIS AOD product at 3-km resolution (MOD04\_3K). The results show that AOD retrievals adequately match with AERONET AOD measurements, with 79.56%, 72.69%, 74.71%, and 61.01% of the collections falling within the MOD04\_3K expected error over land [ $\pm(0.05 + 20\%)$ ] for each of the above-listed regions, respectively. The Improved HARLS (I-HARLS) algorithm performs well overall under different surface conditions, but the data quality gradually decreases with the increase in surface reflectance. Moreover, the I-HARLS algorithm is robust with less bias and can provide more detailed aerosol spatial distributions than those provided by the MOD04\_3K AOD product. These results suggest that the I-HARLS algorithm can be used for air-pollution- and climate-related studies at medium or small scales.

### 1. Introduction

Atmospheric aerosols play an important role in the Earth's environment and climate change from local to global scales; in particular, fine particles have a great influence on human health (Li et al., 2011; Solomon et al., 2007; Sun, Wei, Duan, et al., 2016). Therefore, a comprehensive understanding and discussion of the effects of aerosols on the environment and climate are important. Satellite remote sensing has provided an effective way to analyze the spatial distributions and variations of aerosols on long-term and large scales by detecting their main optical properties, such as aerosol optical depth (AOD) and Ångström exponent ( $\alpha$ ).

AOD is a measure of scattering or extinction of electromagnetic radiation at a given wavelength due to the presence of aerosols in the atmospheric column. For aerosol retrieval in passive remote sensing, the basic principle is to separate the contributions of the atmosphere and the Earth's surface from satellite-received signals. The most critical step is to accurately determine the surface reflectance. Previous studies showed that 1% estimation errors in surface reflectance could lead to approximately 10% errors in aerosol retrieval when the land surface reflectance (LSR) is less than 0.04; when the LSR increases, estimation errors increase by more than 15% with the same 1% inaccurate estimations for surface reflectance (Kaufman, Tanré, et al., 1997; Wei et al., 2017). For dark-target areas (e.g., vegetation and ocean), surface reflectance can be more accurately estimated due to their homogeneous surfaces and low surface-reflectance characteristics. However, for

bright surfaces (e.g., urban areas, arid/semiarid areas, and deserts) other than snow/ice, the sensitivity of aerosol change to top-of-atmosphere (TOA) reflectance decreases with an increase in the LSR. Additionally, diverse underlying surfaces complicate the accurate estimation of LSR and increase the uncertainty of aerosol retrievals (Hsu et al., 2004; Li et al., 2009; Sun et al., 2015; Wei et al., 2017).

Kaufman, Tanré, et al. (1997) and Kaufman, Wald, et al. (1997) found that the LSR over dense vegetation and dark soils was low in blue and red channels and showed nearly fixed ratios with the reflectance at 2.1  $\mu\text{m}$ . Thus, the LSR of blue and red channels could be estimated by the TOA reflectance at 2.1  $\mu\text{m}$ , which was minimally affected by atmospheric aerosols, and the Dark Target (DT) algorithm was developed. Later, the second-generation operational DT algorithm was developed with several main improvements, in which the LSR values of visible channels are estimated via improved dynamic empirical relationships with the TOA reflectance at 2.1  $\mu\text{m}$  related to the normalized difference vegetation index (NDVI) calculated from the short-wave infrared channels ( $\text{NDVI}_{\text{SWIR}}$ ) and scattering angles (Levy, Remer, & Dubovik, 2007; Levy, Remer, Mattoo, et al., 2007; Levy et al., 2010). The DT algorithm can perform well over dark-target surfaces but not over bright surfaces. However, Hsu et al. (2004, 2006) found that the LSR remained low and stable in deep blue channels over deserts and that the AOD could be retrieved if the LSR could be accurately estimated. The Deep Blue (DB) algorithm was proposed, in which the LSRs for visible channels are obtained from a precalculated seasonal LSR database using the Sea-Viewing Wide Field-of-View Sensor surface reflectance products. An Enhanced DB algorithm was further developed based on several main improvements, including surface reflectance estimation, by adopting three approaches for estimating the LSR over vegetated areas, urban areas, and arid and semiarid regions; aerosol model assumption; and cloud screening schemes (Hsu et al., 2013).

MODerate resolution Imaging Spectroradiometer (MODIS) sensors were successfully launched onboard the Terra and Aqua satellites in December 1999 and May 2002, respectively, and the second-generation operational DT algorithm (for land and ocean; Levy et al., 2010) and the Enhanced DB algorithm (only for land; Hsu et al., 2013) have been the main aerosol retrieval algorithms and have produced long-term and global-coverage daily DT and DB AOD products at a spatial resolution of 10 km since collection (C) 6 (MOD04\_10K; Levy et al., 2013). MOD04\_10K AOD products have been extensively evaluated over land and widely used in studies of atmospheric aerosols from local to global scales (Bilal et al., 2013, 2014; Levy et al., 2013; Li et al., 2007; Wei et al., 2017; Wei & Sun, 2017). However, analyses of the spatial distributions and variations of atmospheric pollutants in small- and medium-scale areas are limited due to their coarse spatial resolutions (Bilal et al., 2013; Li et al., 2005; Wei et al., 2018). Therefore, recently, a new global-coverage daily aerosol product at a higher spatial resolution of 3 km (MOD04\_3K) has been released (Remer et al., 2013).

Moreover, an increasing number of researchers have begun to focus on aerosol retrieval at high spatial resolutions to improve the applications in monitoring the air quality and related aerosol studies at urban or local regions. Li et al. (2005) modified the MODIS algorithm to retrieve AODs at 1-km resolution over Hong Kong, and the results showed that the retrievals exhibited low errors in Sun photometer measurements and showed much better correlations with  $\text{PM}_{10}$  measurements than did MOD04 AOD products. Wong et al. (2010) proposed a refined aerosol retrieval algorithm and derived AODs from MODIS at a 500-m resolution with good overall accuracies over Hong Kong and the Pearl River Delta. Lyapustin et al. (2011) put forward a new Multi-Angle Implementation of the Atmospheric Correction (MAIAC) algorithm based on a time series of MODIS images to retrieve AODs over both dark and bright surfaces at 1-km resolution. Bilal et al. (2013) developed a Simplified Aerosol Retrieval Algorithm (SARA) to retrieve AODs from MODIS images at 500-m resolution, and the MOD09GA level 2 daily surface reflectance product was used to provide the surface reflectance for the green channel without using a look-up table (LUT). Although these algorithms can produce reliable aerosol data sets, they can be applied only to specific areas with low universality due to excessive dependence on assumptions and measured input parameters (i.e., surface reflectance and aerosol types). Therefore, it is necessary to explore a more suitable aerosol retrieval method at the global scale, which is the main purpose of this study.

Previous studies showed that the estimation of LSR for aerosol retrieval based on available high-quality atmospheric corrected surface reflectance products could achieve high accuracy over bright areas at a high spatial resolution (Sun et al., 2010, 2015). Typically, current research is undertaken using the high-resolution aerosol retrieval algorithm with a priori LSR database support (HARLS), which was developed

by Wei and Sun (2017) to retrieve aerosols over the Beijing-Tianjin-Hebei region from MODIS images at 1-km resolution. The retrievals were more accurate and less biased than the operational MOD04\_10K AOD products against AEROSOL ROBOTIC NETWORK (AERONET) AOD ground-based measurements. Thus, this study was based on the proposed HARLS algorithm, which was developed for urban areas and then modified and validated for aerosol retrieval at the global scale. For the Improved HARLS (I-HARLS) algorithm, several main improvements were implemented: (1) an estimation of surface reflectance over land, which was based on two distinct approaches for densely vegetated and bright surfaces; (2) an assumption of aerosol types over land, which was based on a precalculated seasonal database combining operational MOD04 aerosol-type data sets and historical records of AERONET optical properties measurements; and (3) cloud screening, which was based on our proposed Universal Dynamic Threshold Cloud Detection Algorithm (UDTCDA; Sun, Wei, Wang, et al., 2016). The AERONET version 2 Level 2.0 AOD measurements were selected to verify the accuracy of retrievals. The following sections introduce the study area and data sets, methodology, results, and discussion.

## 2. Study Area and Data Sources

### 2.1. Typical Local Regions

To test and validate the adaptability of the I-HARLS algorithm, four typical regions—central and eastern Europe (42°N–59°N, 0–16°E; Figure 1a), central and eastern North America (30°N–50°N, 80°W–100°W; Figure 1b), Beijing-Tianjin-Hebei (39°N–41°N, 115°E–118°E; Figure 1c), and the Sahara (12°N–40°N, 14°W–16°E; Figure 1d)—were selected to perform the aerosol retrieval experiments. Europe is dominated by a temperate marine climate and dense vegetation coverage at low elevations. The region has faced environmental pressures in recent years due to air pollution, where the major sources originate from industrial and agricultural production. Aerosols are dominated by fine particles with weak and moderate absorptions (Li et al., 2013). North America has a complex and diverse climate with dense vegetation coverage, and it contains abundant mineral resources with a strong industrial base. Air pollution is inevitable due to early unreasonable industrial development, and the dominant air pollutants are fine particles with weak absorption (Li et al., 2013). Beijing-Tianjin-Hebei is located in eastern China with a large and dense population; the region has experienced increasing air pollution in recent years due to its unreasonable industrial layout and structural pollution and has been a hot spot for urban aerosol retrieval. Aerosols are dominated by fine modes with weak or moderate absorptions (Bilal et al., 2014; Wei et al., 2018; Wei & Sun, 2017). The Sahara is dominated by an arid subtropical climate with low vegetation cover and sparse human activities; it frequently experiences sandy and dusty weather, and the aerosols are dominated by dust, where the distributions of dust particles extensively vary spatially and temporally because of their short lifetime (Hsu et al., 2004; Li et al., 2013). Figure 1 shows the locations of the four typical selected regions.

### 2.2. Data Introduction

#### 2.2.1. Operational MODIS Products

The MOD09 surface reflectance product is an estimate of the surface spectral reflectance in seven channels, from visible to shortwave infrared wavelengths, as it would have been measured at ground level with no atmospheric scattering or absorption. The MOD09 product has been corrected for the effects of atmospheric gases, aerosols, and thin cirrus clouds. The LSR is inverted with the radiative transfer model using atmospheric inputs taken from the National Centers for Environmental Prediction (including ozone and pressure) or directly derived from MODIS products. The atmospheric correction accuracy is  $[\pm(0.005 + 5\%)]$  under favorable conditions (Kotchenova et al., 2006; Kotchenova & Vermote, 2007; Vermote, El Saleous, et al., 1997; Vermote, Tanré, et al., 1997; Vermote, et al., 2002). MOD09A1 is the eight-day synthetic surface reflectance product composited from the MOD09GA daily surface reflectance products. Each pixel contains the best possible observation during an eight-day period as selected based on high observation coverage, low view angle, absence of clouds and cloud shadows, bidirectional reflectance distribution function effects, and aerosol loadings (Vermote & Vermeulen, 1999). In this paper, MOD09A1 products were selected to construct the LSR database.

To monitor the atmospheric particle pollution at medium or small scales, the National Aeronautics and Space Administration has released a global daily aerosol product at 3 km (MOD04\_3K) based on the second-generation DT aerosol retrieval algorithm. This product is based on the same assumptions for

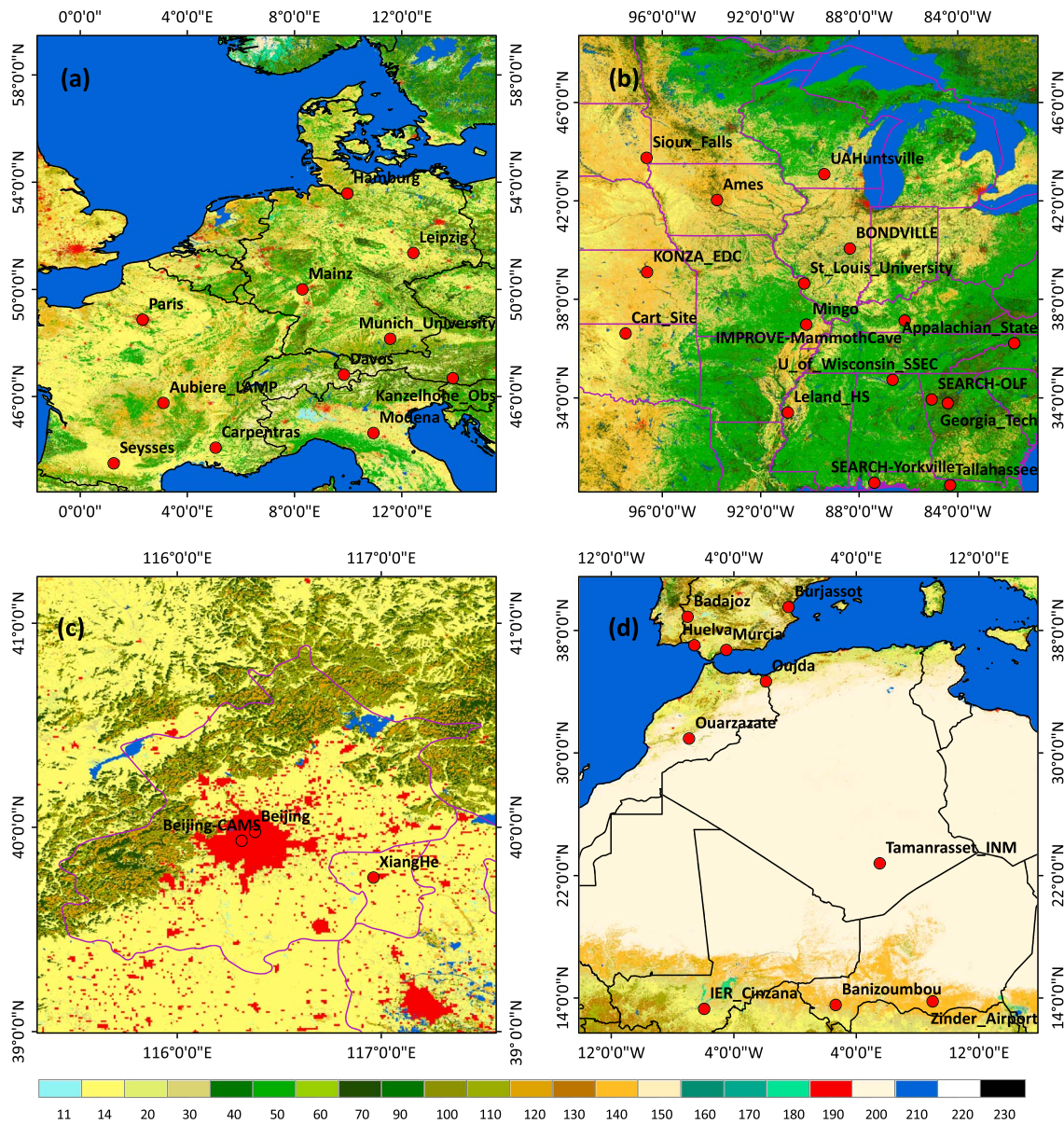


**Figure 1.** Locations of selected typical regions: (a) Europe, (b) North America, (c) Beijing-Tianjin-Hebei, and (d) the Sahara. The red spots represent the AERONET sites. Black and purple solid lines represent the national and state borders, respectively. Land use cover is provided by ESA GlobCover at 300-m spatial resolution. The descriptions of the land use classes in the legend are given in Table S1.

surface reflectance and aerosol types, LUTs, numerical inversion, and criteria to determine a good fit as used in the 10-km product (Levy et al., 2013). The main differences between the two products are the way the pixels are organized and the number of pixels required in the retrieval window during the pixel selection. For the MOD04\_3K DT algorithm, pixels are organized into  $6 \times 6$  pixels in the retrieval box; the 20% darkest and 50% brightest pixels over land are discarded, and then the measured TOA reflectance of remaining pixels are averaged. The algorithm requires a minimum of 5 pixels over land to make a retrieval (Remer et al., 2013). The MOD04 3-km product is expected to resolve aerosol gradients and pollution sources that are missed with the 10-km product. Because there are more selected pixels in the deselection process at 10 km, dark or bright pixels discarded at 10 km might be retained at 3 km, which makes the 3-km product potentially noisier than the 10-km product. Thus, the expected error (EE) for the MOD04 3-km product over land is  $[\pm(0.05\% + 20\%)]$ , which is slightly less

**Table 1**  
Statistical Summary of Data Sets Used in This Study

Data Set	Scientific Data Set (SDS) Name	Contents	Resolutions
MOD021KM	EV_500_Aggr1km_RefSB	Calibrated radiances Height	Daily, 1 km Daily, 1 km
MOD04_3K	Image_Optical_Depth_Land_And_Ocean	DT AOD (QA = 3)	Daily, 3 km
MOD04_10K	Aerosol_Type_Land	Aerosol type	Daily, 10 km
MOD09A1	Surface reflectance bands 1–7	Surface reflectance	8 days, 500 m
AERONET	Version 2, level 2.0	AOD, $\omega_0$ , and $g$	15 min/monthly, –

stringent than that of  $[\pm(0.05\% + 15\%)]$  for the 10-km product over land (Levy et al., 2013; Nichol & Bilal, 2016; Remer et al., 2013). A quality assurance (QA) data set is provided to represent the data quality of AOD retrievals, with QA values ranging from 0 to 3 in order from low to high accuracy (Levy et al., 2013). In this paper, MOD04\_3K DT AOD retrievals with the highest quality (QA = 3) were selected for comparison.

### 2.2.2. AERONET Ground-Based Measurements

AERONET is a worldwide network of calibrated ground-based aerosol sites where observations were collected using the CE-318 Sun photometer measurement. This network has provided a long-term, continuous, and accessible public database of optical properties (i.e., AOD, size distribution, single scattering albedo, and asymmetry parameter) in diverse aerosol regimes. AODs are measured at a wide range of wavelengths from visible to near-infrared channels (0.34–1.02  $\mu\text{m}$ ) every 15 min with a low uncertainty of 0.01–0.02. The AOD measurements are computed as three data quality levels (L): L1.0 (unscreened), L1.5 (cloud screened), and L2.0 (cloud screened and quality assured), indicating increasing reliability (Holben et al., 2001; Smirnov et al., 2000).

In this paper, AERONET version 2 level 2.0 AOD measurements were selected to quantitatively evaluate the reliability of the AOD retrievals. To this end, we collected 11, 16, 3, and 10 AERONET sites over the Europe, North America, Beijing-Tianjin-Hebei, and the Sahara, respectively. The spatial locations and site information of each AERONET site are shown in Figure 1 and Tables 2–5 in the supporting information. However, AERONET does not provide AOD measurements at 550 nm; therefore, they are interpolated with the Ångström exponent algorithm based on the available AOD measurements at the two nearest wavelengths among 440, 500, and 675 nm to compare them with the satellite AOD retrievals (Levy, Remer, & Dubovik, 2007; Sun et al., 2015; Wei et al., 2018, 2017; Wei & Sun, 2017). Table 1 shows a summary of the data sets used in this paper.

## 3. Methodology

An improved high-spatial-resolution (1 km) aerosol retrieval algorithm with prior land surface parameters database support (I-HARLS) for MODIS images over land is proposed. The I-HARLS algorithm requires the TOA reflectance, latitude, longitude, solar zenith/azimuth angles, satellite zenith/azimuth angles, and elevation, which were obtained from MOD02 images at 1-km spatial resolution (MOD021KM). The surface reflectance and aerosol types over land were determined from MODIS surface reflectance (MOD09) products and aerosol (MOD04) products, respectively.

The TOA reflectance received from the satellites contains information from both the atmosphere and surface reflectance and is a function of successive orders of radiation interactions within the coupled surface-atmosphere system, which can be estimated as follows (Tanré et al., 1988; Vermote, El Saleous, et al., 1997):

$$\rho^*(\theta_s, \theta_v, \varphi) = \rho_{Aer}(\theta_s, \theta_v, \varphi) + \rho_{Ray}(\theta_s, \theta_v, \varphi) + \frac{\rho}{1 - \rho^*S} T(\theta_s) T(\theta_v) \quad (1)$$

where  $\rho_{Aer}(\theta_s, \theta_v, \varphi)$  is the aerosol reflectance resulting from multiple scattering in the absence of molecules;  $\rho_{Ray}(\theta_s, \theta_v, \varphi)$  is the multiple Rayleigh reflectance in the absence of aerosols;  $\rho$  is the surface reflectance;  $S$  is the atmospheric backscattering ratio;  $T(\theta_s)$  is the transmission of the atmosphere along the Sun-surface path;  $T(\theta_v)$  is the transmission of the atmosphere along the surface-sensor path; and  $\theta_s$ ,  $\theta_v$ , and  $\varphi$  are the solar zenith angle, view zenith angle, and relative azimuth angle, respectively.

Aerosol reflectance is retrieved at 550 nm by correcting for Rayleigh scattering and the surface function. The aerosol reflectance received from the satellite is a function of the AOD ( $\tau$ ), SSA ( $\omega_0$ ), and aerosol scattering phase function ( $P$ ) as follows:

$$\rho_{Aer}(\theta_s, \theta_v, \varphi) = \frac{\omega_0 \tau P(\theta_s, \theta_v, \varphi)}{4 \cos \theta_s \cos \theta_v} \quad (2)$$

Rayleigh scattering is a notable factor in the radiation calculation and has a significant impact on the visible channels, especially for blue channels (412–490 nm). The Rayleigh scattering correction for satellite data depends on the determination of the Rayleigh phase function and Rayleigh optical depth (ROD; Mishchenko et al., 1999). At sea level, the ROD caused by Rayleigh scattering is a function of wavelength (Bodhaine et al., 1999; Bucholtz, 1995) as follows:

$$\tau_{Ray}(\lambda, z = Z) = 0.00877[\lambda(z = 0) \exp(Z/34)]^{-4.05} \exp(-Z/8.5) \quad (3)$$

where  $\tau_{Ray}$  is the ROD,  $\lambda$  is the wavelength ( $\mu\text{m}$ ),  $z$  is the ground elevation above sea level in kilometers (km), and  $Z$  is the height (km) of the surface target.

The Rayleigh intrinsic reflectance for actual pressure ( $P$ ) is determined by adjusting the molecular optical depth at the standard pressure ( $P_0$ ; 1 atm) level as follows:

$$\tau_{Ray}(\lambda, P) = P / P_0 \tau_{Ray}(\lambda, P_0) \quad (4)$$

The surface reflectance is the most important factor and must be estimated accurately in aerosol retrieval from satellite remote sensing images. Moreover, the composition of global aerosol models is constantly changing in different areas, and aerosol model selection is one of the other key issues in AOD retrieval. Therefore, surface reflectance and aerosol model are two important parameters that affect the accuracy of AOD retrieval and need to be carefully considered.

### 3.1. Surface Reflectance Estimation Over Land

The LSR for vegetated surfaces can vary greatly during growing seasons and remain unchanged for long periods during winter, indicating significant seasonal changes. However, the LSR is relatively high over bright areas (e.g., urban, desert, arid/semiarid, and bare areas), which reduces the sensitivity of aerosol change to TOA reflectance, and no stable relationship between visible and SWIR channels can be estimated. However, the LSRs of bright surfaces do not significantly vary with time, and the effect of the surface's bidirectional reflectance distribution function is weaker than that of vegetated surfaces (Hsu et al., 2013). Therefore, improving LSR estimations for different underlying surfaces requires consideration of dynamic LSR variations. Extensive efforts have focused on these problems, and two typical surface reflectance schemes have been proposed. The pixels over global land are divided into two categories: (1) densely vegetated areas and (2) bright and other areas.

#### 3.1.1. Densely Vegetated Areas

Previous studies showed that the second-generation operational DT algorithm can retrieve stable and accurate AODs for dark-target areas, especially for densely vegetated areas (Levy, Remer, & Dubovik, 2007); thus, the same approach is selected for AOD retrieval over densely vegetated areas in this study. The blue and red channels' LSRs are estimated by the parameters  $\text{NDVI}_{\text{SWIR}}$  and scattering angle. Densely vegetated areas are similarly defined as pixels with  $\text{NDVI}_{\text{SWIR}}$  greater than 0.75, and the LSRs for visible channels can then be estimated (Levy, Remer, & Dubovik, 2007; Levy et al., 2010) as follows:

$$\text{NDVI}_{\text{SWIR}} = \frac{\rho_{1.24}^* - \rho_{2.12}^*}{\rho_{1.24}^* + \rho_{2.12}^*} > 0.75 \quad (5)$$

$$\rho_{0.47} = g(\rho_{0.65}^*) = 0.49\rho_{0.65}^* + 0.005 \quad (6)$$

$$\rho_{0.65} = f(\rho_{2.13}^*) = (0.21 + 0.002\theta)\rho_{2.13}^* - 0.00025\theta + 0.033 \quad (7)$$

$$\theta = \arccos(-\cos \theta_s \cos \theta_v + \sin \theta_s \sin \theta_v \cos \varphi) \quad (8)$$

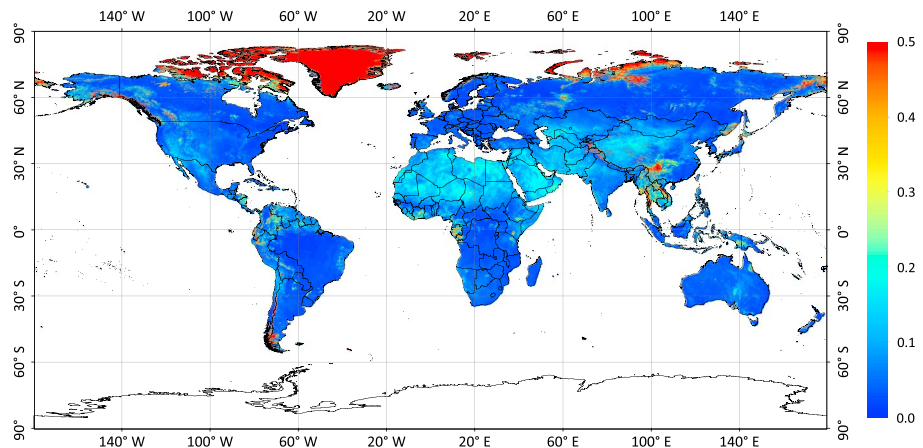


**Figure 2.** Surface reflectance image at the blue ( $0.47 \mu\text{m}$ ) channel on Julian day 161 in 2014 over land.

where  $\rho_{1.24}^*$  and  $\rho_{2.13}^*$  are the TOA reflectance at 1.24 and 2.13  $\mu\text{m}$ , respectively;  $\rho_{0.47}$  and  $\rho_{0.65}$  are the surface reflectance at 0.47 and 0.65  $\mu\text{m}$ , respectively; and  $\theta$  is the scattering angle.

### 3.1.2. Bright and Other Areas

For bright and other surfaces, except for snow/ice surfaces, a new approach is proposed to improve LSR estimations for aerosol retrieval. Carefully considering the LSR variations for vegetated areas at the beginning or end of the growing season, we assume that the LSRs of most features remain unchanged for eight days, and a prior eight-day surface reflectance database is constructed based on the MOD09 series of surface reflectance products. For this purpose, MOD09A1 products encompassing the entire years from 2010 to 2014 are collected and mosaiced to construct a global LSR database.

The database provides 44 LSR images in one year at 1-km resolution. Each LSR image covers four spectral bands, including the blue (459–479 nm), green (545–565 nm), red (620–670 nm), and near-infrared (841–876 nm) channels. Figure 2 provides the LSR images for the blue ( $0.47 \mu\text{m}$ ) channel over land on Julian day 161 in 2014. LSRs are apparently bright in the northern parts of the Northern Hemisphere at relatively high latitudes above  $60^\circ$ , certain tropical regions near the equator, and a few high-altitude areas in the mainland. However, the LSRs in most land areas are relatively low and generally less than 0.15 in the blue channel. Previous studies' simulated results illustrated that the TOA reflectance still responds well to aerosol change even when the surface reflectance is much higher than 0.15 in the blue channel (Sun et al., 2015; Wei et al., 2017). Meanwhile, the LSR image shows an overall high quality with little cloud contamination and can better reflect the LSR variations at the global scale. Therefore, the eight-day synthetic LSR database is used to provide surface reflectance for cloud detection and aerosol retrieval over land.

### 3.2. Assumptions Regarding Aerosol Types Over Land

The composition of global aerosol models is constantly changing in different areas, and aerosol model selection is another key issue in AOD retrievals. Thousands of size distribution retrievals exist, and additional AERONET sites are available around the world. Operational MODIS aerosol products defined aerosol types based on a cluster analysis of all AERONET almuantar and size distribution retrievals in 2005 (Levy, Remer, Mattoo, et al., 2007). Later, a new cluster analysis was performed using AERONET aerosol optical property measurements in 2010. Most AERONET sites remained unchanged in the overall global pattern (Levy et al., 2013). The land aerosol types included a continental model, three fine models, and a dust model. The fine models were separated into strong, moderate, and weak absorption models employing a global map for four seasons.

The key assumptions include the following: the optical properties of each aerosol type vary little spatially over the region during a short time (Bilal et al., 2013; Levy, Remer, Mattoo, et al., 2007; Levy et al., 2013; Sun, Wei, Wang, et al., 2016), and the dominant aerosol type at each site is a function of the season (Levy, Remer, Mattoo, et al., 2007; Levy et al., 2013; Sun, Wei, Jia, et al., 2016; Wei et al., 2018). Thus, a prior seasonal aerosol-type database over land is constructed. For this purpose, MOD04\_10K daily aerosol-type data sets from 2012 to 2014 are collected and used to construct the aerosol-type database. The mode value of aerosol types for

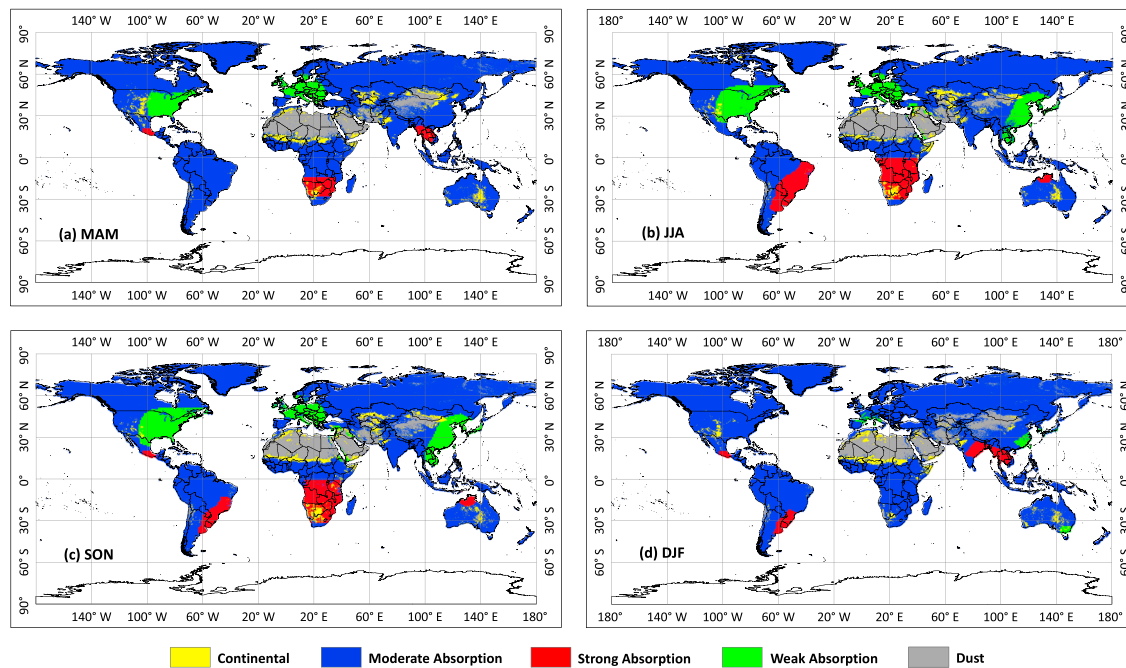


**Figure 3.** Spatial distribution of aerosol types over land in (a) MAM, (b) JJA, (c) SON, and (d) DJF.

each pixel in all images in one season is chosen to represent the pixel for the one-season series. Then, the synthesized seasonal images are further corrected by aerosol optical properties measured by the AERONET ground-based observations at the same time. The database provides four aerosol-type images for each season at 1-km spatial resolution, containing the continental model, moderate absorption model, strong absorption model, weak absorption model, and dust model.

Figure 3 displays the four seasonal land aerosol-type images over land in March-April-May, June-July-August, September-October-November, and December-January-February. The database first provides similar spatial patterns but clearer boundaries of different aerosol types over land compared to that used in the MODIS official aerosol retrieval algorithm (Levy, Remer, Mattoo, et al., 2007; Levy et al., 2013). The aerosol types are as expected in most areas in different seasons. Continental aerosols dominate northern Africa, central Asia, and central Australia. Weakly absorbing aerosols (including urban and industrial aerosols) dominate eastern North America, western Europe, and Southeast Asia, especially in summer and autumn. Strongly absorbing aerosols (including presumably savanna or grassland smoke aerosols) dominate the savannas in South America and Africa. The rest of the world is dominated by moderately absorbing aerosols (including background, forest-smoke, and developing-world aerosols). The optical properties (i.e.,  $\omega_0$  and  $g$ ) of five aerosol models at visible wavelengths are determined from monthly averages of AERONET measurements (Sun, Wei, Jia, et al., 2016).

### 3.3. Cloud Screening

The success of an official MODIS aerosol retrieval depends on its ability to discard unsuitable pixels, including clouds, snow, and inland water bodies. The most critical step for aerosol retrieval is accurate cloud detection to mask unsuitable pixels. Failure to remove clouds from images can create cloud contamination, and an excessively strong cloud mask produces insufficient aerosol coverage. The MOD35 cloud mask product is designed to mask pixels that are unsuitable for land surface retrieval (clouds and heavy aerosol loads) and to find suitable pixels for cloud-product retrieval (not aerosols); MOD35 is viewed as overly cloud conservative but not clear-sky conservative enough for aerosol retrieval (Levy et al., 2013; Sun, Wei, Wang, et al., 2016).

The major challenge in cloud detection is identifying thin and broken clouds over land surfaces, particularly in low- or bright-reflectance areas, which create ubiquitous mixed pixels in the remote sensing images. The difficulty in separating real land surfaces from clouds is the primary reason for the failure to detect thin or



broken clouds with high accuracy from satellite remote sensing images. If the surface reflectance is known, the underlying surface component in mixed pixels can be determined, and the thresholds for cloud detection can be established. Therefore, the Universal Dynamic Threshold Cloud Detection Algorithm (UDTCDA), which is supported by a prior surface reflectance database, is selected to solve the above problems. The dynamic cloud detection models for the visible to near-infrared channels are built based on the simulated relationships between TOA reflectance and surface reflectance. Validations and comparisons with Cloud-Aerosol Lidar and Infrared Pathfinder Satellite Observation cloud measurements and MODIS cloud mask products indicated that it could more accurately detect different kinds of clouds (Sun, Wei, Wang, et al., 2016). Therefore, the UDTCDA for MODIS images is selected to filter pixels for aerosol retrieval in this paper, which are described as follows:

$$\rho_B^{*'} = 0.793\rho_B + 0.004 \cos\theta_s \cos\theta_v + 0.158 \quad (9)$$

$$\rho_G^{*'} = 0.807\rho_G + 0.025 \cos\theta_s \cos\theta_v + 0.125 \quad (10)$$

$$\rho_R^{*'} = 0.843\rho_R + 0.017 \cos\theta_s \cos\theta_v + 0.112 \quad (11)$$

$$\rho_{NIR}^{*'} = 0.928\rho_{NIR} + 0.010 \cos\theta_s \cos\theta_v + 0.099 \quad (12)$$

$$C_i = \rho_i^* - \rho_i^{*'} > 0 \ \& \ NDSI = \frac{\rho_{0.56}^* - \rho_{1.64}^*}{\rho_{0.56}^* + \rho_{1.64}^*} < 0.4, \ i = B, G, R, NIR, \text{ and} \quad (13)$$

$$Cloud = C_B \cup C_G \cup C_R \cup C_{NIR} \quad (14)$$

where represents the simulated TOA reflectance of the blue (B), green (G), red (R), and near-infrared (NIR) channels;  $\rho_i$  and  $\rho_i^*$  represent the surface reflectance and TOA reflectance, respectively, where  $\rho_i$  is obtained from the prior surface reflectance database;  $C_i$  represents the cloud detection results for different channels; NDSI represents the normalized difference snow index (Salomonson & Appel, 2004), where  $\rho_{0.56}^*$  and  $\rho_{1.64}^*$  are the TOA reflectance at 0.56 and 1.64  $\mu\text{m}$ , respectively; and *Cloud* represents the final UDTCDA cloud result.

### 3.4. AOD Retrieval

Similarly, our algorithm uses the LUT approach to provide parameters as MOD04 aerosol retrieval algorithms for AOD retrieval with the Second Simulation of the Satellite Signal in the Solar Spectrum (6S) radiative transfer model (Vermote, Tanné, et al., 1997). The parameters in equation (1) are calculated for different aerosol loadings from 0.0 to 3.0. The TOA reflectance is calculated for solar and sensor zenith angles from 0 to 60° at intervals of 6° and relative azimuth angles from 0° to 180° in increments of 12°. The LUTs contain five aerosol types in tropical (30°S–30°N), midlatitude (30°N–60°N, 30°S–60°S) summer/winter, and subarctic (>60°N, >60°S) summer/winter atmospheric models, which can be determined via the latitudes. The effective retrieval pixels should meet the following conditions: (1) ensure that all the values (i.e., angles and reflectance) are valid; (2) identify and mask most clouds with the UDTCDA algorithm; and (3) identify and mask snow/ice and inland water via the NDSI and normal difference water index (NDWI; Gao, 1996), respectively. Moreover, due to permanent snow/ice or water cover in the polar regions, our algorithm is not designed to retrieve aerosols over areas with high latitudes (>80°S or 80°N).

## 4. Results and Discussion

MOD021KM images covering Europe, North America, and the Sahara during 2012–2014 and Beijing-Tianjin-Hebei during 2010–2014 are downloaded to perform aerosol retrieval experiments. In addition, the AERONET version 2, level 2.0 ground-based AOD measurements and MOD04\_3K AOD products with the same period are collected for validation and comparison. AOD retrievals within a common sampling window of 5 × 5 pixels around the AERONET site are obtained. To remove the AOD retrievals with large fluctuations and less

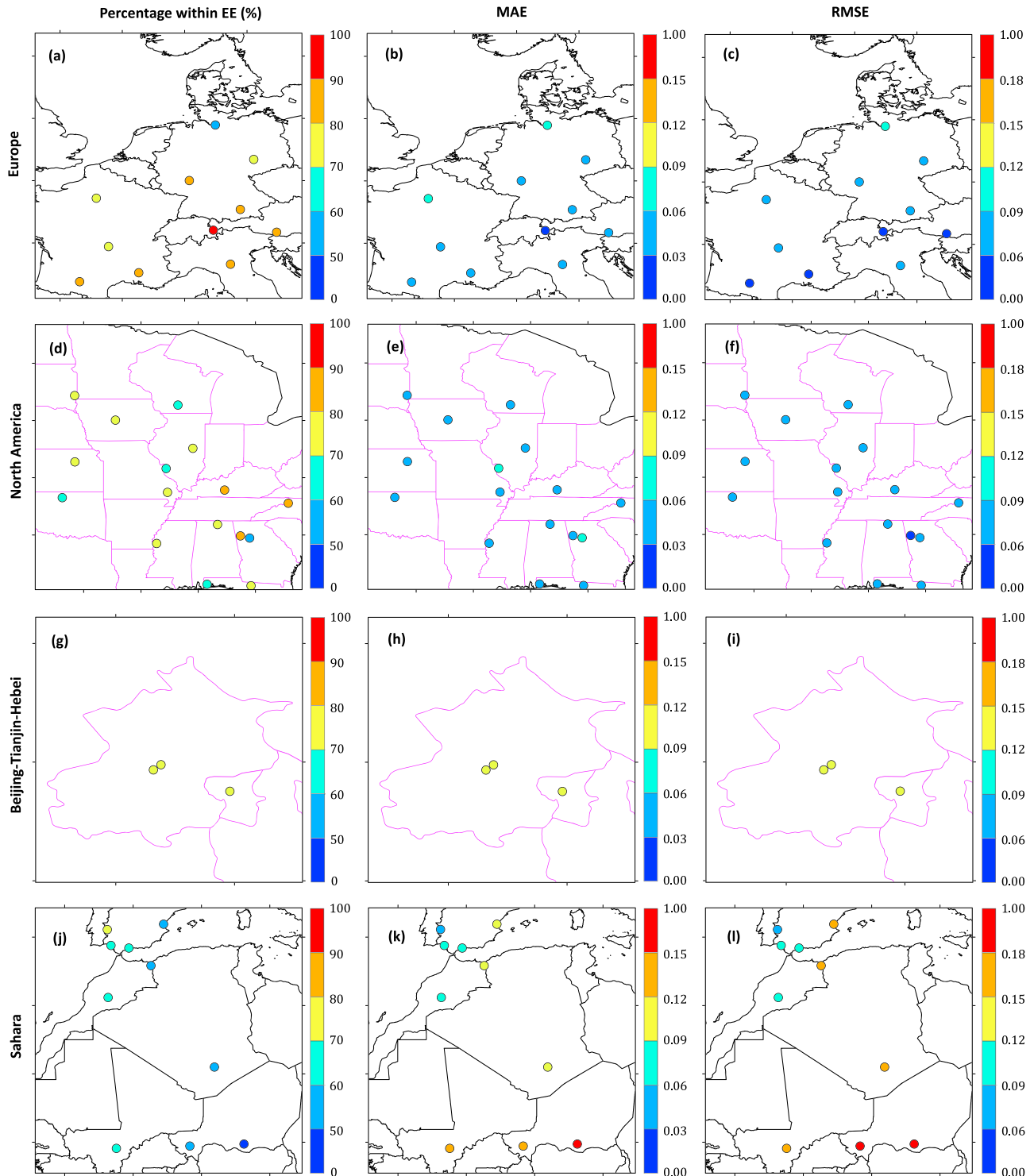


**Figure 4.** Spatial distributions of validations of I-HARLS AOD retrievals with AERONET AOD measurements in the percentages of retrievals falling within the EE (%), MAE, and RMSE at each site over (a–c) Europe, (d–f) North America, (g–i) Beijing-Tianjin-Hebei, and (j–l) the Sahara.

reliability, the 20% highest and 20% lowest pixels are discarded, and the remaining values are averaged as the retrieved AOD. Then, the average of at least two AERONET AOD measurements at each site within  $\pm 30$  min of the MODIS satellites' overpass time are calculated as the true value (Bilal et al., 2014; Hsu et al., 2013; Levy et al., 2013; Wei et al., 2018, 2017). To quantify the accuracy, three main evaluation metrics,

**Table 2**  
Statistical Summary for Validation of I-HARLS AOD Retrievals Over Four Typical Regions and Land

Region	N	R	MAE	RMSE	=EE	>EE	<EE
Europe	1264	0.865	0.050	0.069	79.59	18.51	01.90
North America	1439	0.817	0.052	0.072	72.69	23.49	03.82
Beijing-Tianjin-Hebei	1273	0.943	0.090	0.138	74.71	18.46	06.83
The Sahara	1439	0.774	0.104	0.155	61.01	23.84	15.15
Land	5415	0.913	0.074	0.115	71.67	21.24	07.09

Note. =/>/< EE represent the percentages (%) of retrievals falling within, above, and below the EE, respectively.

including the mean absolute error (MAE), root-mean-square error (RMSE), and EE for the MOD04\_3K AOD product over land [ $\pm(0.05 \pm 20\%)$ ] (Remer et al., 2013) are selected to evaluate the accuracy and uncertainty.

#### 4.1. Validation With AERONET AOD Measurements

##### 4.1.1. Validation at the Site, Regional, and Global Scales

The I-HARLS AOD retrievals at 1-km resolution from MODIS images are first validated against AERONET AODs from 11 sites, 16 sites, 3 sites, and 10 sites over Europe, North America, Beijing-Tianjin-Hebei, and the Sahara, respectively, at both the site and regional scales. Figure 4 provides the spatial distributions of I-HARLS AOD retrievals against AERONET AODs as the percentage of the collections falling within the EE (%), MAE, and RMSE for each site (accuracy statistics

for each site are provided in Tables S2–S5). Table 2 shows the accuracy statistics for Europe, North America, Beijing-Tianjin-Hebei, and the Sahara.

For European sites, more than 70% of the retrievals meet the requirements of the EE at 10 out of 11 AERONET sites, with average MAE and RMSE values less than 0.06 and 0.09, respectively. However, the Hamburg site shows an overall low accuracy, with 58.46% of the collections falling within the EE and average large MAE and RMSE values of 0.079 and 0.102, respectively. The main reason is that the high-latitude location (53.57°N) and the effects of snow/ice in winter increase the difficulties in estimating the surface reflectance. Moreover, despite good accuracies, AOD retrievals show overall low overestimation uncertainties at most sites (Figures 4a–4c and Table S2). At the regional scale, a total of 1,264 effective points are collected, and they agree well with AERONET AODs ( $R = 0.865$ ), with 79.59% of the retrievals falling within the EE, and average small MAE and RMSE values of 0.050 and 0.069, respectively (Table 2).

The I-HARLS algorithm shows overall good performance over North America at the site scale; more than 60% of the retrievals fall within the EE at 15 out of 16 selected sites, with average MAE and RMSE values less than 0.06 and 0.09, respectively. Despite this, AOD retrievals show certain overestimation uncertainties at most sites (Figures 4d–4f and Table S3). At the regional scale, we collect a total of 1,439 points; they are highly correlated with the AERONET AODs ( $R = 0.917$ ), and 72.69% of them meet the requirements of the EE with an average MAE of 0.052 and RMSE of 0.072 (Table 2).

In Beijing-Tianjin-Hebei, 563, 150, and 560 pairs are collected for Beijing, Beijing\_CAMS, and XiangHe sites, respectively. For two typical urban sites (Beijing and Beijing\_CAMS), the I-HARLS AOD retrievals agree well with AERONET AODs ( $R = 0.941$  and  $0.950$ ), and 70.52% and 72.67% of the retrievals fall within the EE, with average MAEs of 0.092 and 0.096 and RMSEs of 0.134 and 0.148, respectively. Moreover, the highest accuracy

is found for the XiangHe site, which is located in the suburbs and covered by vegetation, with 79.46% of the collections falling within the EE, and the retrievals agree well with AERONET AOD measurements with an average MAE of 0.086 and RMSE of 0.139, respectively (Figures 4g–4i and Table S4). Despite the good accuracies, the estimation uncertainty (i.e., MAE and RMSE) increases compared to those in Europe and North America. In general, we collect a total of 1,273 pairs from three sites, and they are highly correlated with AERONET AOD measurements; 74.71% of them meet the requirements of the EE, with an average MAE of 0.09 and RMSE of 0.138 (Table 2). Furthermore, the overall data qualities of I-HARLS AOD retrievals are obviously improved over those of HARLS AOD retrievals, with 65.41%, 58.95%, and 70.16% of the collections falling within the EE for Beijing, Beijing\_CAMS, and XiangHe sites, respectively, as reported in a previous study (Wei & Sun, 2017). This approach improves estimations for surface reflectance and assumptions for aerosol types.

For the Sahara, the I-HARLS algorithm performs poorly at most sites. Only half of the 10 selected sites show considerable accuracies, with more than 60% of collections falling within the EE, showing high

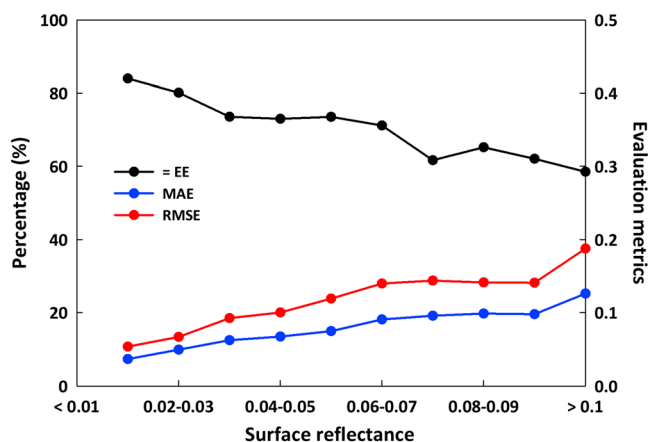


**Figure 5.** Performance of the I-HARLS algorithm as a function of surface reflectance, where = EE represent the percentages (%) of retrievals falling within the EE.

**Table 3**  
Statistical Summary for Validation of I-HARLS AOD Retrievals for Different Aerosol Types

Aerosol type	N	R	MAE	RMSE	=EE	>EE	<EE
Continental	140	0.788	0.138	0.194	57.14	22.86	20.00
Moderate absorption	3186	0.937	0.074	0.113	72.13	21.85	06.02
Weak absorption	1473	0.848	0.050	0.069	77.12	21.05	01.83
Dust	616	0.759	0.120	0.175	59.58	18.18	22.24

estimation uncertainties with large MAE and RMSE values. Especially for the sites located deep in the Sahara desert, AOD retrievals are poorly correlated with the AERONET AOD measurements, with larger average MAE and RMSE values exceeding 0.09 and 0.15, respectively (Figures 4j–4l and Table S5). The main reason is the decreasing sensitivity of aerosols changes to TOA reflectance with the increasing surface reflectance over such bright desert surfaces. At the regional scale, a total of 1,439 points are collected, and they show good agreements with AERONET AODs ( $R = 0.771$ ); 61.1% of them fall within the EE, with an average MAE of 0.104 and RMSE of 0.155 (Table 2). These

results illustrate that the aerosol estimation uncertainty for the Sahara is greater than those for Europe, North America, and Beijing-Tianjin-Hebei.

For the whole land, we have collected 5,415 effective data pairs across all selected 40 sites from four typical regions. It is found that our 1-km I-HARLS AOD retrievals are highly consistent ( $R = 0.913$ ) with AERONET AOD measurements at 550 nm over land. The retrievals are evenly distributed on both sides of the 1:1 line with average MAE and RMSE values of 0.074 and 0.115, respectively. In general, the I-HARLS algorithm performs well, with approximately 71.67% of the retrievals falling within the EE, at the global scale over land (Table 2).

#### 4.1.2. Influence of Surface Reflectance and Aerosol Type on Retrievals

The above analysis shows that there are significant differences in the performances of aerosol retrieval at both site and regional scales; these differences are mainly related to the surface reflectance and aerosol types. Therefore, to further explore the effects of both factors on aerosol retrieval, we classify the AERONET sites into several groups under different surface reflectance conditions and aerosol types according to the precalculated land surface reflectance and aerosol-type images. The corresponding I-HARLS AOD retrievals are validated against the AERONET AOD measurements.

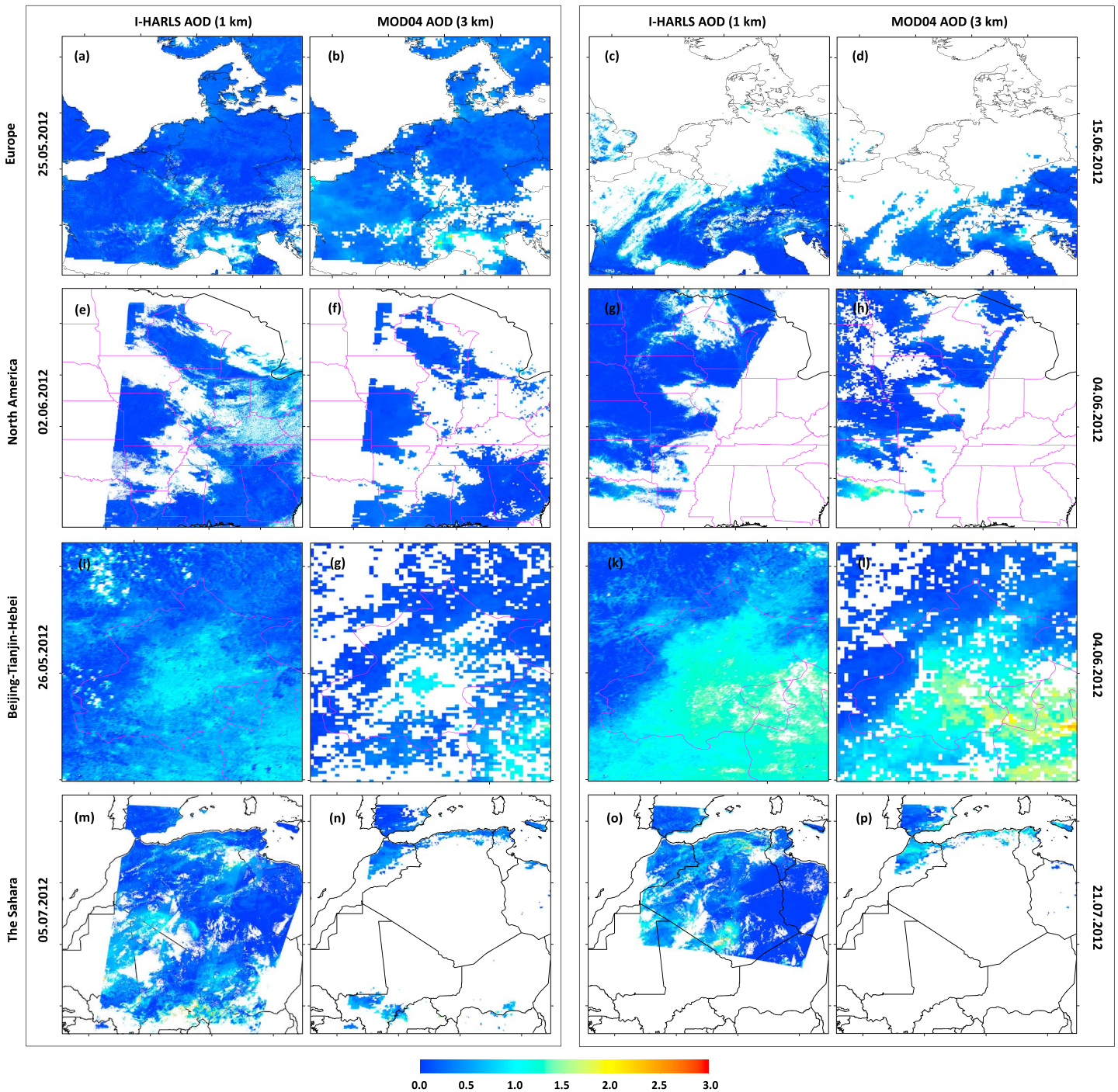
Figure 5 illustrates the performances of the I-HARLS AOD retrievals along with the increasing surface reflectance from 0.0 to 0.1 at an interval of 0.01 (Table S6), indicating the validations from the darkest to brightest surfaces. The results demonstrate that the aerosol retrievals show good performance at low surface reflectance less than 0.07, and they agree well with AERONET AODs ( $R = 0.867$ – $0.935$ ). More than 70% of the collections fall within the EE, showing overall small MAE ranges from 0.03 to 0.10, and the RMSE values range from 0.05 to 0.14. The reason is that in the low-surface-reflectance areas, LSRs are easier to determine. However, when the surface reflectance continues to increase, the percentages of retrievals falling within the EE gradually decline and the estimation errors increase. This pattern occurs because with an increase in surface reflectance, surface information becomes complex, and the sensitivity of aerosol change to TOA reflectance decreases, increasing the difficulties in estimating the surface reflectance and leading to low-quality retrievals (Wei et al., 2018).

Table 3 shows the accuracy statistics of the performances of AOD retrievals for different aerosol types. The new algorithm shows different performances for various aerosol types. In areas dominated by moderately and weakly absorbing aerosols, which occupied most of the continent, the I-HARLS algorithm performs well overall, with 72.12% and 77.12% of the collections falling within the EE, respectively. The average MAE values are 0.074 and 0.050, and RMSE values are 0.113 and 0.069, respectively. There is no obvious difference (~5%) between the areas dominated by these two aerosol types. However, in continental- and dust-aerosol-dominated areas, mainly located in parts of the continent and deserts characterized by great depth, it performs poorly, with approximately 57.14% and 59.58% of the retrievals falling within the EE, respectively. The average MAE and RMSE values are greater than 0.12 and 0.17, respectively, mainly because of the common influence of uncertainties in estimating the surface reflectance and assuming the aerosol type over such areas.

## 4.2. Comparison With MOD04\_3K AOD Products

### 4.2.1. Spatial Distributions Among Different MODIS Aerosol Products

For this paper, eight images obtained in 2012 on 25 May and 15 June over Europe, 2 and 4 June over North America, 26 May and 4 June over Beijing-Tianjin-Hebei, and 5 and 21 July over the Sahara are selected to display the aerosol spatial distributions of the I-HARLS (1-km) and MOD04 (3-km) AOD products (Figure 6). The I-



**Figure 6.** Comparisons of spatial distributions of I-HARLS AOD (1 km) with MOD04\_3K AOD (3 km) over Europe, North America, Beijing-Tianjin-Hebei, and the Sahara on selected days (dd.mm.yyyy). The solid black line represents national borders, and the purple solid line represents state/provincial borders.

HARLS AODs show consistent spatial distributions similar to those of the MOD04\_3K AOD products over Europe (Figures 6a–6d) and North America (Figures 6e–6h), where low aerosol loadings have always been observed. However, I-HARLS AODs could provide wider spatial coverage than MOD04\_3K AODs, mainly due to a more accurate cloud mask, given that the MOD04 cloud masks used in the aerosol retrieval overestimated the cloud fraction in the images (Sun, Wei, Wang, et al., 2016). Over bright urban surfaces, the MOD04\_3K AOD products show a large number of missing values with poor spatial continuity in central

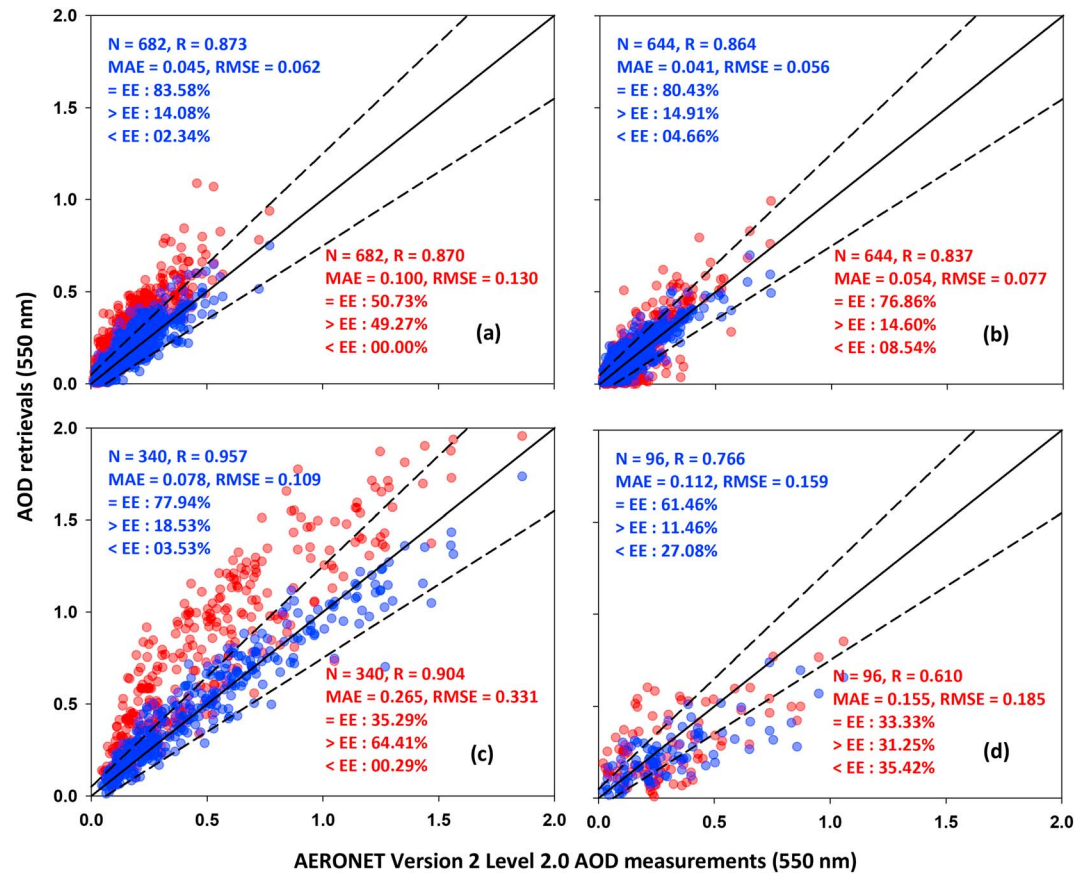


**Figure 7.** Comparisons of common AOD collections between I-HARLS (1 km) and MOD04\_3K AOD retrievals (3 km) against AERONET AOD measurements over (a) Europe, (b) North America, (c) Beijing-Tianjin-Hebei, and the (d) Sahara. The blue and red dots represent I-HARLS and MOD04\_3K AOD retrievals, respectively, and  $\neq$ / $>$ / $<$  EE represent the percentages (%) of AOD retrievals falling within, above, and below the EE, respectively.

urban areas, while the I-HARLS algorithm could achieve aerosol retrieval in such areas and provide more constant spatial coverage. The MOD04\_3K AODs are always higher than I-HARLS AODs in such areas. In addition, in the surrounding vegetated areas, they show close and continuous spatial coverage (Figures 6i–6l). Furthermore, in the deserts, the MOD04\_3K AODs show few successful retrievals because the DT algorithm could not achieve aerosol retrievals over such bright surfaces with high surface reflectance; in contrast, the I-HARLS algorithm could achieve much more successful retrievals and provide more constant spatial coverage over the Sahara (Figures 6m–6p). More importantly, the I-HARLS AOD product has a higher spatial resolution at 1 km than does the MOD04\_3K AOD product, indicating that it can provide more detailed aerosol spatial distributions and variabilities over land.

#### 4.2.2. Comparison With MOD04\_3K AOD Products

For comparison purposes, the MOD04\_3K AOD retrievals passing the highest-quality assurance (QA = 3) are obtained for four regions. Figure 7 illustrates the validation and comparison of common retrievals between I-HARLS and MOD04\_3K AOD products against AERONET AODs, and Table 4 provides the statistical summary of validation for unique I-HARLS AOD retrievals during 2010–2014 for four typical regions over land.

In Europe, a total of 682 common AOD retrievals for I-HARLS and MOD04\_3K AOD products are collected from all sites. The MOD04\_3K AODs show close agreements with the AERONET AOD measurements ( $R = 0.870$ ), yet only 50.73% of them fall within the EE, with an

**Table 4**

Statistical Summary for Validation of Unique I-HARLS AOD Retrievals Over Four Typical Regions

Region	N	R	MAE	RMSE	=EE	>EE	<EE
Europe	582	0.866	0.056	0.075	75.04	23.59	01.37
North America	795	0.807	0.062	0.083	66.42	30.44	03.14
Beijing-Tianjin-Hebei	933	0.941	0.093	0.146	72.97	19.13	07.90
The Sahara	1343	0.780	0.103	0.154	60.98	24.72	14.30

average MAE of 0.100 and RMSE of 0.130. However, serious overestimations with almost half of the collections (49.27%) falling above the EE are observed. Compared to MOD04\_3K AODs, the I-HARLS AODs achieve a higher correlation with AERONET AODs ( $R = 0.873$ ) and an average lower MAE of 0.045 and RMSE of 0.062. Meanwhile, this algorithm can significantly reduce the overestimation uncertainties. In general, 83.55% of the collections fall within the EE, which is approximately 1.65 times greater than that of MOD04\_3K AOD retrievals (Figure 7a). Furthermore, 582 unique AOD pairs are collected from I-HARLS AOD product, and they are also highly correlated with AERONET AODs, with 75.04% of these collections falling within the EE and average MAE and RMSE values of 0.056 and 0.075, respectively.

In North America, a total of 644 common AOD retrievals between the I-HARLS and MOD04\_3K AOD products are collected from all sites. MOD04\_3K AOD retrievals show good performance with a high correlation of 0.864 with AERONET AODs, and approximately 76.86% of the collections fall within the EE, with an average MAE of 0.054 and RMSE of 0.077. However, the I-HARLS AOD retrievals achieve a high correlation with AERONET AODs ( $R = 0.837$ ), and more than 80% of them fall within the EE with an average lower MAE of 0.041 and RMSE of 0.056, showing an overall improvement in the aerosol estimations (Figure 7b). Moreover, another 795 unique AOD pairs for I-HARLS retrievals are collected and validated against AERONET AOD measurements. The retrievals agree well with the measurements ( $R = 0.807$ ), and 66.42% of them are within the EE, with an average MAE of 0.062 and RMSE of 0.083.

Similarly, common retrievals between I-HARLS and MOD04\_3K AOD products are extracted, but only 340 effective pairs are obtained in the Beijing-Tianjin-Hebei region. MOD04\_3K AODs exhibit poor performance, and only 35.29% of the retrievals fall within the EE, with an average MAE of 0.265 and RMSE of 0.331. Moreover, this algorithm significantly overestimates the aerosol loadings, with more than 64% of the retrievals falling above the EE. However, the I-HARLS algorithm is able to largely reduce the overestimation uncertainties and significantly improve the data quality over this region. The percentage of the retrievals falling within the EE increases to 77.94%, which is approximately 2.2 times more than that of the MOD04\_3K retrievals. The retrievals are highly correlated with the AERONET AODs and show much lower average MAE of 0.078 and RMSE of 0.109 (Figure 7c). Furthermore, 962 additional AOD pairs are collected from the I-HARLS retrievals, and they agree well with the AERONET AODs; approximately 73% of them are within the EE, showing average MAE and RMSE values of 0.093 and 0.146, respectively.

The common retrievals between the I-HARLS and MOD04\_3K products are extracted from all sites over the Sahara. More serious is that only 96 effective points are obtained, and the MOD04 AOD retrievals show poor performance over the Sahara, with only 33.33% of them falling within the EE and an average MAE of 0.155 and RMSE of 0.185. Similarly, serious estimation uncertainties are observed with 31% and 35% of the retrievals falling above and below the EE, respectively. There are no common retrievals from the desert sites, Tamanrasset\_INM and Ouarzazate, which is mainly because the MOD04\_3K DT algorithm is unable to retrieve AODs over such bright desert surfaces. However, the I-HARLS algorithm performs much better than the MOD04 DT algorithm, and more than 61.46% of the common retrievals fall within the EE, with decreasing MAE and RMSE values of 0.112 and 0.159, respectively (Figure 7d). Moreover, a large number of 1343 unique AOD pairs are collected from the I-HARLS retrievals, and they correlate well with the AERONET AODs, with 60.98% of them falling within the EE and an average MAE of 0.103 and RMSE of 0.154. The comparison results show that the I-HARLS algorithm allows aerosol retrieval from darkest to brightest surfaces, and it not only increases the number of successful retrievals but also improves the aerosol estimations.

## 5. Conclusions

In this paper, an improved high-spatial-resolution aerosol retrieval algorithm with land surface parameter support (I-HARLS) at 1-km resolution for MODIS images is developed. A precalculated global land surface reflectance (LSR) database is constructed using the MODIS eight-day synthetic surface reflectance (MOD09A1) products, and a prior seasonal global land aerosol-type database is created using the MOD04 daily aerosol products. The main aerosol optical properties and types are determined based on the monthly average historical aerosol optical properties from local AEROSOL ROBOTIC NETWORK (AERONET) sites. For cloud screening, the Universal Dynamic Cloud Detection Algorithm (UDTCDA) is selected to mask cloud pixels in remote sensing images. Then, a 1-km-resolution AOD data set is generated based on the I-HARLS

algorithm. Successful AOD retrievals are available over dark and bright surfaces. To test and validate the performance of the I-HARLS algorithm, four typical regions (including Europe, North America, Beijing-Tianjin-Hebei, and the Sahara) with different underlying surface and aerosol types are selected for aerosol retrieval experiments. Moreover, AERONET version 2, level 2.0 AOD measurements and MODIS daily AOD products at 3-km resolution (MOD04\_3K) are selected for validations and comparisons.

The results show that the I-HARLS algorithm performs well overall at both the site and regional scales, and AOD retrievals are highly correlated with AERONET AOD measurements, with 79.56%, 72.69%, 74.71%, and 61.01% of the collections falling within the EE for the four regions, respectively. However, with an increase in surface reflectance over land, the overall performance of the retrievals decreases with increasing estimation errors, mainly due to the decreasing sensitivity of aerosol change to TOA reflectance. The new AOD products perform better and are less biased than the MOD04\_3K AOD product, primarily because of the improvements in LSR estimation and aerosol-type assumption. Furthermore, the generated 1-km-resolution AOD data sets can provide continuous and wide-spatial-coverage AOD distributions over land, which play an important role in quantitative aerosol research and air quality monitoring at the medium and small scales.

This study shows that although the new AOD retrieval algorithm performs well overall over land, certain problems remain. Due to the large amount of data, four representative local regions with three or five years of data are selected for this paper for aerosol retrieval experiments and validations. However, due to the long time series of MODIS data records, longer and wider-scale experiments and validations need to be undertaken. In addition, this paper only performs comparisons with current operational and free-open high-resolution MOD04 aerosol products; therefore, more comprehensive and effective comparison efforts with other high-resolution products (such as MAIAC products) need to be performed in future studies.

#### Acknowledgments

The MODIS products are available from the Goddard Space Flight Center Level 1 and Atmosphere Archive and Distribution System (<http://ladsweb.nascom.nasa.gov>), and AERONET measurements are available from the NASA Goddard Space Flight Center (<https://aeronet.gsfc.nasa.gov/>). This work was supported by the National Natural Science Foundation of China (41171408 and 41761144056) and the National Science Foundation of Shandong Province (ZR201702210379). All authors made substantial contributions to this work. Jing Wei designed the experiments and wrote the paper; Lin Sun, Yiran Peng, Lunche Wang, Zhaoyang Zhang, and Muhammad Bilal helped review the paper; and Yanci Ma helped collect and process the satellite data. We declare no conflict of interest. The Editor and three anonymous reviewers are thanked for their helpful comments, which have improved the manuscript. Here I want to thank my wife for her support and for bringing me our first child in my life.

#### References

- Bilal, M., Nichol, J. E., Bleiweiss, M. P., & Dubois, D. (2013). A simplified high resolution MODIS aerosol retrieval algorithm (SARA) for use over mixed surfaces. *Remote Sensing of Environment*, *136*, 135–145. <https://doi.org/10.1016/j.rse.2013.04.014>
- Bilal, M., Nichol, J. E., & Chan, P. W. (2014). Validation and accuracy assessment of a simplified aerosol retrieval algorithm (SARA) over Beijing under low and high aerosol loadings and dust storms. *Remote Sensing of Environment*, *153*, 50–60. <https://doi.org/10.1016/j.rse.2014.07.015>
- Bodhaine, B. A., Wood, N. B., Dutton, E. G., & Slusser, J. R. (1999). On Rayleigh optical depth calculations. *Journal of Atmospheric and Oceanic Technology*, *16*(11), 1854–1861. [https://doi.org/10.1175/1520-0426\(1999\)016<1854:ORODC>2.0.CO;2](https://doi.org/10.1175/1520-0426(1999)016<1854:ORODC>2.0.CO;2)
- Bucholtz, A. (1995). Rayleigh-scattering calculations for the terrestrial atmosphere. *Applied Optics*, *34*(15), 2765–2773. <https://doi.org/10.1364/AO.34.002765>
- Gao, B. C. (1996). NDWI—A normalized difference water index for remote sensing of vegetation liquid water from space. *Remote Sensing of Environment*, *58*(3), 257–266. [https://doi.org/10.1016/S0034-4257\(96\)00067-3](https://doi.org/10.1016/S0034-4257(96)00067-3)
- Holben, B. N., Tanré, D., Smirnov, A., Eck, T. F., Slutsker, I., Abuhassan, N., Newcomb, W. W., et al. (2001). An emerging ground-based aerosol climatology: Aerosol optical depth from AERONET. *Journal of Geophysical Research*, *106*(D11), 12,067–12,097. <https://doi.org/10.1029/2001JD900014>
- Hsu, N. C., Jeong, M. -J., Bettenhausen, C., Sayer, A. M., Hansell, R., Seftor, C. S., Huang, J., et al. (2013). Enhanced deep blue aerosol retrieval algorithm: The second generation. *Journal of Geophysical Research: Atmospheres*, *118*, 9296–9315. <https://doi.org/10.1002/jgrd.50712>
- Hsu, N. C., Tsay, S. -C., King, M. D., & Herman, J. R. (2004). Aerosol properties over bright reflecting source regions. *IEEE Transactions on Geoscience and Remote Sensing*, *42*(3), 557–569. <https://doi.org/10.1109/TGRS.2004.824067>
- Hsu, N. C., Tsay, S. -C., King, M. D., & Herman, J. R. (2006). Deep blue retrievals of Asian aerosol properties during ACE-Asia. *IEEE Transactions on Geoscience and Remote Sensing*, *44*(11), 3180–3195. <https://doi.org/10.1109/TGRS.2006.879540>
- Kaufman, Y. J., Tanré, D., Gordon, H. R., Nakajima, T., Lenoble, J., Frouin, R., Grassl, H., et al. (1997). Passive remote sensing of tropospheric aerosol and atmospheric correction for the aerosol effect. *Journal of Geophysical Research*, *102*(D14), 16,815–16,830. <https://doi.org/10.1029/97JD01496>
- Kaufman, Y. J., Wald, A. E., Remer, L. A., Gao, B.-C., Li, R.-R., & Flynn, L. (1997). The MODIS 2.1- $\mu\text{m}$  channel-correlation with visible reflectance for use in remote sensing of aerosol. *IEEE Transactions on Geoscience and Remote Sensing*, *35*(5), 1286–1298. <https://doi.org/10.1109/36.628795>
- Kotchenova, S. Y., & Vermote, E. F. (2007). Validation of a vector version of the 6S radiative transfer code for atmospheric correction of satellite data. Part II. Homogeneous Lambertian and anisotropic surfaces. *Applied Optics*, *46*(20), 4455.
- Kotchenova, S. Y., Vermote, E. F., Matarrese, R., & Klemm, F. J. (2006). Validation of a vector version of the 6S radiative transfer code for atmospheric correction of satellite data. Part I: Path radiance. *Applied Optics*, *45*(26), 6762–6774. <https://doi.org/10.1364/AO.45.006762>
- Levy, R. C., Mattoo, S., Munchak, L. A., Remer, L. A., Sayer, A. M., Patadia, F., & Hsu, N. C. (2013). The collection 6 MODIS aerosol products over land and ocean. *Atmospheric Measurement Techniques*, *6*(11), 2989–3034. <https://doi.org/10.5194/amt-6-2989-2013>
- Levy, R. C., Remer, L. A., & Dubovik, O. (2007). Global aerosol optical properties and application to Moderate Resolution Imaging Spectroradiometer aerosol retrieval over land. *Journal of Geophysical Research*, *112*, D13210. <https://doi.org/10.1029/2006JD007815>
- Levy, R. C., Remer, L. A., Kleidman, R. G., Mattoo, S., Ichoku, C., Kahn, R., & Eck, T. F. (2010). Global evaluation of the collection 5 MODIS dark-target aerosol products over land. *Atmospheric Chemistry and Physics Discussions*, *10*(6), 14815–14873. <https://doi.org/10.5194/acpd-10-14815-2010>



- Levy, R. C., Remer, L. A., Mattoo, S., Vermote, E. F., & Kaufman, Y. J. (2007). Second-generation operational algorithm: Retrieval of aerosol properties over land from inversion of Moderate Resolution Imaging Spectroradiometer spectral reflectance. *Journal of Geophysical Research*, *112*, D13211. <https://doi.org/10.1029/2006JD007811>
- Li, C., Lau, K. H., Mao, J., & Chu, D. A. (2005). Retrieval, validation, and application of the 1-km aerosol optical depth from MODIS measurements over Hong Kong. *IEEE Transactions on Geoscience and Remote Sensing*, *43*(11), 2650–2658.
- Li, Y., Xue, Y., de Leeuw, G. D., Li, C., Yang, L., Hou, T., & Marir, F. (2013). Retrieval of aerosol optical depth and surface reflectance over land from NOAA AVHRR data. *Remote Sensing of Environment*, *133*(133), 1–20. <https://doi.org/10.1016/j.rse.2013.01.020>
- Li, Z., Niu, F., Fan, J., Liu, Y., Rosenfeld, D., & Ding, Y. (2011). Long-term impacts of aerosols on the vertical development of clouds and precipitation. *Nature Geoscience*, *4*(12), 888–894. <https://doi.org/10.1038/ngeo1313>
- Li, Z., Zhao, X., Kahn, R., Mishchenko, M., Remer, L., Lee, K.-H., Wang, M., et al. (2009). Uncertainties in satellite remote sensing of aerosols and impact on monitoring its long-term trend: A review and perspective. *Annals De Geophysique*, *27*(7), 2755–2770. <https://doi.org/10.5194/angeo-27-2755-2009>
- Li, Z. Q., Niu, F., Lee, K. H., Xin, J. Y., Hao, W. M., Nordgren, B., Wang, Y., et al. (2007). Validation and understanding of moderate resolution imaging spectroradiometer aerosol products (C5) using ground-based measurements from the handheld Sun photometer network in China. *Journal of Geophysical Research*, *112*, D22507. <https://doi.org/10.1029/2007JD008479>
- Lyapustin, A., Wang, Y., Laszlo, I., Kahn, R., Korokin, S., Remer, L., Levy, R., et al. (2011). Multi-angle implementation of atmospheric correction (MAIAC): 2. Aerosol algorithm. *Journal of Geophysical Research*, *116*, D03211. <https://doi.org/10.1029/2010JD014986>
- Mishchenko, M. I., Geogdzhayev, I. V., Cairns, B., Rossow, W. B., & Laci, A. A. (1999). Aerosol retrievals over the ocean by use of channels 1 and 2 AVHRR data: Sensitivity analysis and preliminary results. *Applied Optics*, *38*(36), 7325–7341. <https://doi.org/10.1364/AO.38.007325>
- Nichol, J., & Bilal, M. (2016). Validation of MODIS 3 km resolution aerosol optical depth retrievals over Asia. *Remote Sensing*, *8*(4), 328. <https://doi.org/10.3390/rs8040328>
- Remer, L. A., Mattoo, S., Levy, R. C., & Munchak, L. A. (2013). MODIS 3 km aerosol product: Algorithm and global perspective. *Atmospheric Measurement Techniques*, *6*(7), 1829–1844. <https://doi.org/10.5194/amt-6-1829-2013>
- Salomonson, V. V., & Appel, I. (2004). Estimating fractional snow cover from MODIS using the normalized difference snow index. *Remote Sensing of Environment*, *89*(3), 351–360. <https://doi.org/10.1016/j.rse.2003.10.016>
- Smirnov, A., Holben, B. N., Eck, T. F., Dubovik, O., & Slutsker, I. (2000). Cloud screening and quality control algorithms for the AERONET database. *Remote Sensing of Environment*, *73*(3), 337–349. [https://doi.org/10.1016/S0034-4257\(00\)00109-7](https://doi.org/10.1016/S0034-4257(00)00109-7)
- Solomon, S., Qin, D., Manning, M., Marquis, M., Averyt, K., Tignor, M. M. B., et al. (Eds) (2007). *Climate Change 2007: The Physical Science Basis*. Cambridge: Cambridge University Press.
- Sun, L., Sun, C. K., Liu, Q. H., & Bo, Z. (2010). Aerosol optical depth retrieval by HJ-1/CCD supported by MODIS surface reflectance data. *Chinese science. Earth Science*, *53*(s1), 74–80.
- Sun, L., Wei, J., Bilal, M., Tian, X., Jia, C., Guo, Y., & Mi, X. T. (2015). Aerosol optical depth retrieval over bright areas using Landsat 8 OLI images. *Remote Sensing*, *8*(1), 23. <https://doi.org/10.3390/rs8010023>
- Sun, L., Wei, J., Duan, D. H., Guo, Y. M., Yang, D. X., Jia, C., & Mi, X. T. (2016). Impact of land-use and land-cover change on urban air quality in representative cities of China. *Journal of Atmospheric and Solar-Terrestrial Physics*, *142*, 43–54. <https://doi.org/10.1016/j.jastp.2016.02.022>
- Sun, L., Wei, J., Jia, C., Yang, Y. K., Zhou, X. Y., et al. (2016). *A High-Resolution Global Dataset of Aerosol Optical Depth Over Land From MODIS Data* (pp. 5729–5732). Beijing, China: 2016b IEEE International Geoscience and Remote Sensing Symposium (IGARSS). <https://doi.org/10.1109/IGARSS.2016.7730497>
- Sun, L., Wei, J., Wang, J., Mi, X., Guo, Y., Lv, Y., et al. (2016). A universal dynamic threshold cloud detection algorithm (UDTCDA) supported by a prior surface reflectance database. *Journal of Geophysical Research: Atmospheres*, *121*, 7172–7196. <https://doi.org/10.1002/2015JD024722>
- Tanré, D., Deschamps, P. Y., Devaux, C., & Herman, M. (1988). Estimation of Saharan aerosol optical thickness from blurring effects in thematic mapper data. *Journal of Geophysical Research*, *93*(D12), 15,955–15,964. <https://doi.org/10.1029/JD093iD12p15955>
- Vermote, E. F., El Saleous, N., Justice, C. O., Kaufman, Y. J., Privette, J. L., Remer, L., Roger, J. C., et al. (1997). Atmospheric correction of visible to middle-infrared EOS-MODIS data over land surfaces: Background, operational algorithm and validation. *Journal of Geophysical Research*, *102*(D14), 17,131–17,141. <https://doi.org/10.1029/97JD00201>
- Vermote, E. F., El Saleous, N. Z. E., & Justice, C. O. (2002). Atmospheric correction of MODIS data in the visible to middle infrared: First results. *Remote Sensing of Environment*, *83*(1-2), 97–111. [https://doi.org/10.1016/S0034-4257\(02\)00089-5](https://doi.org/10.1016/S0034-4257(02)00089-5)
- Vermote, E. F., Tanré, D., Deuzé, J. L., Herman, M., & Morcette, J.-J. (1997). Second simulation of the satellite signal in the solar spectrum, 6S: An overview. *IEEE Transactions on Geoscience and Remote Sensing*, *35*(3), 675–686. <https://doi.org/10.1109/36.581987>
- Vermote, E. F. & Vermeulen, A. (1999). Atmospheric correction algorithm: Spectral reflectances (MOD09). Algorithm Theoretical Background Document, version 4.0.
- Wei, J., Huang, B., Sun, L., Zhang, Z., Wang, L., & Bilal, M. (2017). A simple and universal aerosol retrieval algorithm for Landsat series images over complex surfaces. *Journal of Geophysical Research: Atmospheres*, *122*, 13,338–13,355. <https://doi.org/10.1002/2017JD026922>
- Wei, J., & Sun, L. (2017). Comparison and evaluation of different MODIS aerosol optical depth products over the Beijing-Tianjin-Hebei region in China. *IEEE Journal of Selected Topics in Applied Earth Observations and Remote Sensing*, *10*(3), 835–844. <https://doi.org/10.1109/JSTARS.2016.2595624>
- Wei, J., Sun, L., Huang, B., Bilal, M., Zhang, Z., & Wang, L. (2018). Verification, improvement and application of aerosol optical depths in China part 1: Inter-comparison of NPP-VIIRS and aqua-MODIS. *Atmospheric Environment*, *175*, 221–233. <https://doi.org/10.1016/j.atmosenv.2017.11.048>
- Wong, M. S., Lee, K. H., Nichol, J. E., & Li, Z. (2010). Retrieval of aerosol optical thickness using MODIS, a study in Hong Kong and the Pearl River Delta region. *IEEE Transactions on Geoscience and Remote Sensing*, *48*(8), 3318–3327. <https://doi.org/10.1109/TGRS.2010.2045124>